JOURNAL OF COMPUTATIONAL PHYSICS 96, 297–324 (1991)

Spectral Methods for the Navier–Stokes Equations with One Infinite and Two Periodic Directions

PHILIPPE R. SPALART, ROBERT D. MOSER, AND MICHAEL M. ROGERS

NASA Ames Research Center, Moffett Field, California 94035

Received March 23, 1990; revised October 1, 1990

Two numerical methods were designed to solve the time-dependent, three-dimensional, incompressible Navier–Stokes equations in boundary layers (method A, semi-infinite domain) and mixing layers or wakes (method B, fully-infinite domain). Their originality lies in the use of rapidly-decaying spectral basis functions to approximate the vertical dependence of the solutions, combined with one (method A) or two (method B) slowly-decaying "extra functions" for each wave-vector that exactly represent the irrotational component of the solution at large distances. Both methods eliminate the pressure term as part of the formulation, thus avoiding fractional-step time integration. They yield rapid convergence and are free of spurious modes in the Orr–Sommerfeld spectra. They are also efficient, although the operation count is of order N^2 (N is the number of modes in the infinite direction). These methods have been used for extensive direct numerical simulations of transition and turbulence. A new time-integration scheme, with low storage requirements and good stability properties, is also described. © 1991 Academic Press, Inc.

1. INTRODUCTION

The numerical solution of the full Navier–Stokes equations is becoming a mature field and is contributing to the theoretical and quantitative knowledge of transition and turbulence, at least in simple geometries. A review and references can be found in [1]. Most of the direct numerical simulations (DNS) of turbulent flows have been performed with spectral methods in Cartesian coordinates with various boundary conditions in each direction [2–3]. Periodic conditions are the easiest and most often used boundary conditions, leading to Fourier series expansions which are accurate and efficient. The only difficulty regarding Fourier methods is the treatment of aliasing errors for nonlinear or variable-coefficient equations. In the case of a finite interval with "physical" boundary conditions, such as the no-slip condition, polynomial basis functions are most often used because they are accurate and lead to efficient algorithms [1–3]. Incompressible viscous solutions and their derivatives are expected to be smooth so Fourier series or polynomials yield rapid convergence. There are several treatments of the boundary conditions, including the Galerkin method, the τ method, and the collocation method, all of which are commonly implemented with polynomial basis functions. The case of a finite interval with inflow–outflow conditions is more delicate, and in our opinion not a good application for a spectral method.

0021-9991/91 $3.00
Copyright © 1991 by Academic Press, Inc.
All rights of reproduction in any form reserved.

Infinite intervals create an additional challenge because even smooth functions that approach a known finite value can have a wide variety of asymptotic behaviors at infinity, different enough to have a major impact on the convergence of the spectral method (or of any numerical method). Let the y direction be the infinite one. In the common situation considered here, there is an "active" region, such as a boundary layer or mixing layer containing vorticity and small eddies, and one or two "freestream" regions in which the velocity smoothly approaches its freestream value (as $|y| \to \infty$). The rate at which this approach occurs (typically algebraic, exponential, or Gaussian) depends on the boundary conditions in the other directions and on the history of the flow. If the basis functions tend to the freestream value faster than the exact solution the accuracy will be poor, just as when the exact solution is discontinuous and the basis functions are not (Gibbs phenomenon, [2]).

Since the freestream conditions in y specify that the velocity must tend to a finite value, polynomials in terms of y are ruled out as basis functions because all nonconstant polynomials are unbounded as $|y| \to \infty$. It is also possible to truncate the solution domain at a large but finite value Y. However, a straightforward polynomial method (without a mapping) would concentrate too much resolution near Y to be efficient. Since a mapping would be needed and because Y is introduced as an extra parameter, there appears to be no advantage to this approach over mapping the infinite domain in y. Another possibility would be to use polynomials of y multiplied by a rapidly-decaying function (such as an exponential). This has not been well explored and it is not clear that it would yield rapid convergence.

The prevailing spectral methods for infinite domains [3–9] are described as "mapping methods," that is, a mapping $y \leftrightarrow \eta$ is defined such that η varies within a finite interval, and the basis functions are polynomials in terms of η. This provides functions that tend smoothly to finite limits as $|y| \to \infty$. Naturally the mapping is singular, in that $d\eta/dy \to 0$ as $|y| \to \infty$. It is a matter of convention whether an algorithm is presented as a mapping method or as one based on the equivalent functions of y. For instance, on $[0, \infty)$ the same method can be viewed as based on polynomials of η, with $\eta \equiv e^{-y}$, or simply as based on the functions e^{-my} (m integer). The mapping presentation has the advantage that many properties of common orthogonal functions (trigonometric, Jacobi, and Chebyshev polynomials) are easily accessible [10] and are used extensively during the design of the methods. This includes algebraic properties such as recursion relations, and analytical properties such as the convergence to smooth functions.

Most of the methods in use rely on mappings which are algebraic in the sense that the asymptotic relationship between y and η as $y \to \infty$ is algebraic. An example is $\eta \equiv y/(1+y)$. Orszag [11], Boyd [5], and Metcalfe *et al.* [8] have strongly advocated algebraic mappings over exponential mappings for solution of the Navier–Stokes equations; they have shown that exponential mappings lead to poor convergence associated with Gibbs phenomena (see Section 3). Both methods presented here use exponential mappings. The poor convergence expected for such methods is avoided by using extra basis functions that take advantage of the

disparate decay rates of the velocity and vorticity. This is possible because the asymptotic form of the velocity for large $|y|$ is known. Depending on the problem, our methods may produce a high but finite order of convergence, instead of the "infinite" order convergence spectral methods are known to achieve in ideal problems. In practice, the rapidity of the *initial* convergence (the number of modes required to obtain a given finite accuracy) is more important than the *asymptotic* rate of convergence (when $N \to \infty$). When considering the initial convergence to error levels important in real computations, the difference between "spectral" and finite but high order accuracy is usually not significant. Both methods described here provide good initial convergence because the exponential mapping concentrates their resolution in the vortical region, where steep gradients and small scales exist.

In Section 2 we cover preliminaries needed in the remainder of the paper, none of which are new [12, 13]. In Section 3 we introduce the extra functions, and the treatment of the nonlinear terms is presented in Section 4. The implementation of method A is then discussed in Section 5, and that of method B in Section 6.

2. Preliminaries

The incompressible Navier–Stokes equations for the velocity vector $\mathbf{U}(x, y, z, t)$ (with components u, v, and w), the vorticity $\boldsymbol{\omega} \equiv \nabla \times \mathbf{U}$ and the total pressure P can be written as

$$\nabla \cdot \mathbf{U} = 0, \tag{1a}$$

$$\frac{\partial \mathbf{U}}{\partial t} + \boldsymbol{\omega} \times \mathbf{U} = -\nabla P + \frac{1}{\mathrm{Re}} \nabla^2 \mathbf{U}. \tag{1b}$$

A velocity U, a length δ, and a pressure ρU^2 have been used to non-dimensionalize (1) and define the Reynolds number, $\mathrm{Re} = U\delta/\nu$ (ν is the kinematic viscosity). This non-dimensionalization is used throughout the paper. Periodic conditions are applied in the x and z directions.

For method A the interval in y is $[0, \infty)$. The no-slip condition at the wall is

$$\mathbf{U}(x, 0, z, t) = \mathbf{U}_w, \tag{2}$$

and the freestream condition is

$$\lim_{y \to +\infty} \mathbf{U} = \mathbf{U}_{+\infty}. \tag{3}$$

For method B the interval is $(-\infty, \infty)$ and the lower condition is

$$\lim_{y \to -\infty} \mathbf{U} = \mathbf{U}_{-\infty}. \tag{4}$$

$\mathbf{U}_w$, $\mathbf{U}_{-\infty}$, and $\mathbf{U}_{+\infty}$ are given and may be time-dependent. Except in wakes, the boundary conditions in y are inhomogeneous; that is, $\mathbf{U}_w \neq \mathbf{U}_{+\infty}$ (A) or $\mathbf{U}_{-\infty} \neq \mathbf{U}_{+\infty}$ (B). It is therefore convenient to define a "base flow" $\mathbf{U}_0$ that satisfies these inhomogeneous conditions and solve for a "disturbance field" $\mathbf{U}_1 \equiv \mathbf{U} - \mathbf{U}_0$. $\mathbf{U}_0$ should be smooth, simple to evaluate and differentiate (normally just a function of y), and satisfy (1a), (2) or (4), and (3). The equations governing $\mathbf{U}_1$ are then easily derived from (1) and $\mathbf{U}_1$ satisfies homogeneous boundary conditions. Neither method discussed here requires pressure boundary conditions, other than periodicity in x and z. However, if $\mathbf{U}_{+\infty}$ is time-dependent a "base pressure" P_0 that has the required jump over one period in x or z needs to be added. It is the disturbance pressure field P_1 ($P_1 \equiv P - P_0$) that is periodic. This is also the standard procedure for channel-flow simulations (e.g., [13]).

Let the $\hat{}$ symbol denote quantities which have been Fourier transformed in both x and z (e.g., $\hat{u}(k_x, y, k_z, t)$). In Fourier space it is natural to decompose each Fourier mode of the velocity vector into a vector "+" and a vector "−" mode, as introduced for cylindrical coordinates in [12], Cartesian coordinates in [13], and spherical coordinates in [14]. Let $k = \sqrt{k_x^2 + k_z^2}$ be the magnitude of the wave-vector (k_x, k_z). Excluding the case $k = 0$ for now we can define the horizontal velocity components parallel and perpendicular to the wave-vector

$$\hat{u}^{\parallel} \equiv \frac{k_x \hat{u} + k_z \hat{w}}{k}, \qquad \hat{u}^{\perp} \equiv \frac{-k_z \hat{u} + k_z \hat{w}}{k}. \tag{5}$$

The continuity equation (in Fourier space: $ik_x \hat{u} + \partial \hat{v}/\partial y + ik_z \hat{w} = 0$) is then

$$ik\hat{u}^{\parallel} + \frac{\partial \hat{v}}{\partial y} = 0. \tag{6}$$

The vector + mode is given by $U^+ = (u^{\parallel}, v, 0)$, while the minus mode is $U^- = (0, 0, u^{\perp})$. The − modes are thus not involved in the continuity equation; the only constraints they need to satisfy are the boundary conditions. Also, they are decoupled from the + modes in the linear terms of the momentum equation (pressure and viscous). Modes with different wave-vectors are also decoupled in the linear operators, as usual. The + modes are two-dimensional modes in the plane containing the wave-vector and the y axis. This decomposition of the velocity amounts to Squire's transformation [15]. The horizontal components of vorticity parallel and perpendicular to the wave-vector are

$$\hat{\omega}^{\parallel} \equiv \frac{k_x \hat{\omega}_x + k_z \hat{\omega}_z}{k}, \qquad \hat{\omega}^{\perp} \equiv \frac{-k_z \hat{\omega}_x + k_x \hat{\omega}_z}{k}, \tag{7}$$

and the solenoidal character of the vorticity is expressed as

$$ik\hat{\omega}^{\parallel} + \frac{\partial \hat{\omega}_y}{\partial y} = 0. \tag{8}$$

In this decomposition, the kinematic relationship between vorticity and velocity is expressed as

$$-ik\hat{u}^{\perp} = \hat{\omega}_y, \tag{9a}$$

$$\frac{\partial^2 \hat{v}}{\partial y^2} - k^2 \hat{v} = ik\hat{\omega}^{\perp}. \tag{9b}$$

When $k=0$, the $+/-$ decomposition is not possible. However, in this case $\hat{v}=\hat{\omega}_y=0$ and $\hat{u}$ and $\hat{w}$ are treated in the same way as $\hat{u}^{\perp}$ (method A) or $\hat{\omega}^{\perp}$ (method B). Note that in this case there is no slowly decaying potential component of velocity and the extra functions described in Section 3 are not needed.

In both methods the solution $\mathbf{U}_1$ is sought as a linear combination of basis functions that satisfy continuity and homogeneous boundary conditions [16]. By virtue of the $+/-$ decomposition, the choice of (vector) expansion functions is reduced to the choice of two sets of scalar functions; one for $\hat{v}$ (and $\hat{u}^{\parallel}$, its derivative by (6)), the other to represent $\hat{u}^{\perp}$. The choice of these functions depends on the method because of the different boundary conditions. Another difference between methods A and B is that in A the Navier–Stokes equations are solved directly for the velocity, while for B the vorticity equations are solved. The reason for the difference is that the no-slip condition at the wall is more easily applied in the velocity formulation of method A while the vorticity formulation of method B is more natural in the absence of walls. In reality the difference between these two formulations is slight (see Section 6.3).

The scalar expansion functions are chosen by first selecting a (exponential) mapping of the infinite domain in y to a finite domain in η. A set of orthogonal polynomials in η are then chosen as the building blocks for the basis functions. The actual basis functions will be a second-degree (methods A and B) or third-degree (method A) polynomial times the orthogonal polynomials, which is done to impose the required boundary conditions. As was the case in the methods of Moser *et al.* [13], these polynomial prefactors also happen to simplify the expression of derivatives.

Chebyshev polynomials have been most often used in spectral methods because of the availability of a "fast" transform with a cost of order $N \log N$ compared to N^2 for a "slow" transform. However, Chebyshev polynomials have the disadvantage that their orthogonality weight function is singular at the boundary and therefore they cannot be used if orthogonality and integration by parts are to be used in evaluating the integrals that arise in a vector Galerkin method (see Section 5.1). Each of the methods presented here uses a (different) member of the class of Jacobi polynomials. They are selected to simplify the expression of the integrals arising from the Galerkin method (see Sections 5.2 and 6.1). Thus the expansion functions have been designed to be optimum for a particular problem, with a particular mapping. The lack of a fast transform imposes a performance penalty when N gets to be large. The value of N at which this becomes burdensome, however, is quite high (about 60 in method A and 120 in method B). There are several reasons for this:

(1) modern super-computer hardware is better suited to computing slow transforms (as matrix multiplies) than fast transforms; (2) the slow transform can include other operations (e.g., computing a derivative), which would otherwise need to be done as a separate step; and (3) even/odd decoupling in method B allows the transforms to be done as two transforms of length $N/2$.

Once the expansion functions are chosen, coupled ordinary differential equations in time are obtained using a Galerkin method. The expansion is substituted into the governing equation, the equation is multiplied in turn by each of the expansion functions and integrated over the spatial domain $\mathscr{D}$. Let the governing equation be given by $\mathcal{O}(\psi)=0$, where $\mathcal{O}$ is a possibly vector-valued, possibly nonlinear operator (e.g., the Navier–Stokes equations), and ψ is a possibly vector function. Having chosen expansion functions (say χ_i), ψ is sought as a linear combination, $\psi=\sum_{i=0}^{N} a_i\chi_i$. The expansion coefficients a_i, which are usually functions of time, are required to satisfy

$$\int_{\mathscr{D}} \chi_j \cdot \mathcal{O}\left(\sum_{i=0}^{N} a_i\chi_i\right) dx = 0 \qquad \text{for} \quad j=0, 1, 2, ..., N. \tag{10}$$

Galerkin methods have favorable properties [3]. In particular, depending on the properties of $\mathcal{O}$, the solution can be shown to be near optimal in the sense that the norm of the error ε in the solution ($\int_{\mathscr{D}} \varepsilon\cdot\varepsilon\, dx$) is near minimum (the error in ψ obtained from (10) is less than some constant times the minimum error possible given the χ_i's and N). This implies that the convergence properties of the method are just the convergence properties for approximation of a known function by the expansion functions. This is the case for linear elliptic operators. For linear parabolic operators (like the Stokes equations) a similar result holds which involves time integrals of the norm of the error. Since the expansions used here are Fourier and polynomial series with known rapid convergence to sufficiently smooth functions, rapid convergence of the methods described here is expected, although we know of no proof of this for the Navier–Stokes equations.

Other desirable properties of the methods presented here are that they eliminate the pressure from the equations and that the representations inherently satisfy all constraints (continuity and boundary conditions). This allowed us to directly obtain ordinary differential equations in time for the expansion coefficients (a_i) without the need for fractional-step time discretization schemes. The time discretization is fully independent of the spatial discretization. The time-advance methods used, including one that is new, are discussed in the Appendix.

3. Extra Functions

In the flows treated here one can distinguish a turbulent, vortical region of thickness δ and an essentially irrotational region above it (and below for method B), usually with a sharp interface between the two. There are several reasons to expect

the interface between the vortical and irrotational regions to be sharp, meaning that the vorticity decays very rapidly as $y \to \infty$. First the flows of interest are at high Reynolds numbers, thus the viscous diffusion which tends to smear the vorticity throughout the domain is very weak. Second, in some cases the vorticity initially decays rapidly in y and the flow is simulated for a relatively short time so this remains the case for the duration of the computation. In other cases the flow is computed for a long time but model terms derived from a multiple-scale procedure are added to the Navier–Stokes equations causing the vorticity to be slowly convected towards the active region, thus counteracting viscous diffusion [17].

As an example, the solutions of the Orr–Sommerfeld equation in a boundary layer which are associated with discrete eigenvalues clearly exhibit two decay rates. If k is the wavenumber and c the phase velocity of the wave, the velocity is found to decay like e^{-ky} whereas the vorticity decays like e^{-Ky}, where $K \approx \sqrt{(1/2)\, k\, \mathrm{Re}\, |\, \|\mathbf{U}_{+\infty}\| - c|}$ [15]. For typical Reynolds numbers and wavenumbers, K is much larger than k (and even much larger than $1/\delta$). This property has been exploited in many Orr–Sommerfeld solvers.

From here on we assume that the vorticity decays exponentially at a rapid rate K as $|y| \to \infty$ (i.e., $\|\boldsymbol{\omega}\| = O(e^{-K|y|})$). In particular, K is much larger than $k_{\min}$, the smallest wavenumber in the simulation ($k_{\min} = 2\pi/\Lambda$, where Λ is the larger of the horizontal period lengths). Usually the wavenumbers involved in a DNS range from values smaller than the most unstable Orr–Sommerfeld wavenumbers to values much larger than $1/\delta$, and possibly larger than K. From the condition $\|\boldsymbol{\omega}\| = O(e^{-K|y|})$ and (9a) it is clear that $\hat{u}^{\perp}$ decays at the same rate as $\|\boldsymbol{\omega}\|$ (i.e., $\hat{u}^{\perp} = O(e^{-K|y|})$). In contrast, integrating (9b) and assuming that $K > k$ yields

$$\hat{v} = Ae^{-k|y|} + O(e^{-K|y|}) \tag{11}$$

(where A is an integration constant) for the asymptotic behavior of $\hat{v}$ as $|y| \to \infty$. This suggests adapting the basis functions of the + modes ($\hat{v}$ and $\hat{u}^{\parallel}$, related by (6)) to the multiple-scale structure of the solution (11). This will allow a good resolution of the "vortical" part, $O(e^{-K|y|})$, and an exact resolution of the "irrotational" part $e^{-k|y|}$, even if they have very different decay rates ($K \gg k$). Note that the form of the irrotational part is known exactly in advance; the only inconvenience is that it depends on the wavenumber. The strategy is the following. A mapping and a set of "regular" basis functions are chosen such that they can resolve functions that are $O(e^{-K|y|})$, and for each wave-vector one (method A) or two (method B) "extra" basis functions which decay like $e^{-k|y|}$ are included in the description to resolve the irrotational part.

The decay rate of the velocity and vorticity is important because we wish to ensure the rapid convergence of our polynomial expansions. In both methods the mapping $y \leftrightarrow \eta$ is asymptotically exponential (e.g., $\eta \sim e^{-y/y_1}$ as $y \to \infty$ for some length scale y_1). The failure of such mappings, as pointed out by Orszag [11], is that the irrotational component e^{-ky} is to leading order η^{ky_1}, with ky_1, in general, noninteger. Such a function cannot be well approximated by polynomials because

its ith derivative with respect to η, where $i-1<ky_1<i$, is singular at $\eta=0$. The error of a polynomial expansion of this function would go as $1/N^i$ [2]. Thus unless ky_1 is large, and especially if it is less than 1, the convergence of an expansion of e^{-ky} will be slow. On the other hand, if the function to be approximated has an infinite number of continuous derivatives, the expansion will converge "spectrally" (i.e., faster than $1/N^i$ for any i). In the current methods an expansion in polynomials in η is sought for only the "vertical part," which is $O(e^{-K|y|})$ for large $|y|$. The parameter y_1 is then chosen so that $Ky_1 \gg 1$, and therefore high-order convergence is obtained. We do not insist on spectral convergence because there are no firm estimates for the decay rate of $\|\omega\|$ and because in practice the difference between high-order (say tenth) and spectral convergence is not significant.

The task of resolving the irrotational part of the solution using only the regular expansion functions has been addressed in at least three ways. Laurien and Kleiser [9] use an exponential mapping and make y_1 large so that $ky_1>1$. Another possibility (as suggested by Jimenez, personal communication) is to use an exponential mapping but adjust y_1 such that ky_1 is an integer for all k (this is only possible in two dimensions). Orszag, on the other hand, uses an algebraic mapping, so that the regular basis functions decay more slowly than e^{-ky} [11]. An algebraic mapping was also adopted by Stanaway *et al.* [14]. These approaches all ignore the multiple-scale nature of the solution (11) and will be increasingly inefficient when larger horizontal periods (compared with the boundary-layer thickness) are used, because they will squander more and more resolution away from the vortical layer itself. In fact, extra functions could improve the initial (if not the asymptotic) convergence of methods based on mappings other than exponential by allowing the length scale of the mapping to scale with the vortical-layer thickness instead of the period.

Including an extra function adds to the complexity of the program and could disrupt the structure of the matrices built around the regular basis functions. In method A this disruption is minimized by the fact that the irrotational component, by nature, is orthogonal to all the other basis functions. Thus it does not add any extra bands or lines in the + mode matrices (see Section 5.2). In method B, the Laplacians of the extra functions are regular basis functions, which also preserves the structure of the matrices. Another concern is the behavior of the method when k is not smaller than K. In that case (11) becomes meaningless; in fact the extra function can then cause numerical difficulties, which will be discussed separately for methods A and B.

4. Treatment of the Nonlinear Terms

In computing the nonlinear terms in a Galerkin method it is necessary to evaluate the integral $\int_{\mathscr{D}} \chi_i \cdot N(\psi)\, dx$, where χ_i is one of the basis functions as in (10) and $N(\psi)$ is the nonlinear term. This is most often done using Gauss quadrature because the availability of fast transforms in at least some spatial directions (e.g.,

fast Fourier transforms) makes it more efficient than performing the convolution sums which would otherwise be required [2]. In the absence of the extra functions, the Gauss quadratures can be made exact by using $\frac{3}{2}$ as many quadrature points as basis functions in the expansions (because the nonlinear term is quadratic). This is what is normally done in both methods.

When the extra functions are included, the velocity cannot be expressed as a finite sum of polynomials in η, so the Gauss quadrature is not guaranteed to be exact. However, it is expected to be very accurate for two reasons. First, we use the rotational form of the nonlinear terms $(\mathbf{U} \times \boldsymbol{\omega})$. When this is multiplied by the test functions (either regular functions or an extra function in method A), the resulting integrand decays at least as fast as the vorticity at infinity. Thus, the approximation of the integrand by polynomials in η, and therefore the value of the integral, should converge rapidly for large N. If a different form of the nonlinear terms were to be used (e.g., $\mathbf{U} \cdot \nabla \mathbf{U}$), the accuracy of the quadrature would be degraded by the slow decay at infinity. Second, in both methods the extra functions (and therefore the velocity) can be expressed as very smooth functions which decay slowly at infinity, plus a finite-order polynomial in η. The Gauss quadrature scheme applied to the polynomial part in the nonlinear terms will be exact. The smooth slowly decaying part, when multiplied by the vorticity in the nonlinear terms, yields a function which is no more difficult to resolve than the vorticity in the active vortical region.

As stated above, we use $\frac{3}{2}$ as many quadrature points as expansion functions to ensure exact (or very accurate) evaluation of the nonlinear term quadratures. The same is done in x and z in which Fourier expansions are used. The errors thus avoided are commonly called aliasing errors. The use of the "$\frac{3}{2}$ rule" to eliminate aliasing is relatively expensive (40% of the cost of a typical boundary layer simulation using method A), and it is a matter of controversy as to whether this is a good use of resources. In turbulence simulations of a boundary layer (performed using method A) and a plane channel (performed using a different spectral method, J. Kim private communication), it has been observed that when dealiasing is discontinued fully-developed turbulence will begin to decay and ultimately die. The computational time required for dealiasing could alternatively be used to refine the computational mesh by increasing the number of modes by about 15% in each coordinate direction. This, however, is still insufficient to ensure that the turbulence does not die. If the flows were very well resolved, there would be no sensitivity to aliasing. However, marginal resolution is a necessity in our attempts to reach (barely) realistic Reynolds numbers. It has been observed that aliasing errors are most damaging when the rotational form of the nonlinear term is used [18]. However, we are required to use the rotational form to ensure an acceptable behavior of the nonlinear terms at infinity for the Gauss quadrature. One final advantage of removing aliasing errors is that it makes the current methods (and many others, e.g., those in [13]) stable even when severely underresolved. The solutions are somewhat inaccurate, but still turbulent. This has been used to advantage to expedite transients by computing to statistical steady state with coarse resolution, and then proceeding with fine resolution [17]. It has also been used to

explore a large parameter space by doing many coarsely resolved simulations; when an interesting solution is found, the simulation can be continued (or repeated) with finer resolution.

5. Method A: Boundary Layers

In this section we consider the Navier–Stokes equations (1) in an infinite domain $[0, \infty)$ in y with boundary conditions (2) and (3).

5.1. *Vector Weighted-Residual Formulations*

Leonard [16] presented a spectral method based on divergence-free basis functions and a weighted-residual formulation of the momentum equation (1b). He mentioned the following advantages over previous methods: exact treatment of the continuity condition and boundary conditions, simpler time-advance scheme (the pressure term is eliminated), and lower storage requirements. The method has most of the advantages of the vorticity-streamfunction methods, but by working with the velocity instead of the vorticity it avoids the difficulties associated with vorticity boundary conditions at a solid wall. The method was applied to a circular pipe by Leonard and Wray [12], to straight and curved channels by Moser *et al.* [13], and to vortex rings by Stanaway *et al.* [14].

The constraints imposed on $\mathbf{U}_1$, namely the continuity condition and the homogeneous boundary conditions, are linear and time-independent; they define a subspace of the space of all possible velocity fields. The search for a solution is restricted to that subspace from the onset. There is an immediate numerical advantage to working in a smaller space in that there are fewer degrees of freedom to follow for a given resolution: two per mode, instead of four when the three velocity components and the pressure are computed.

Once the constraints have been applied the representation acquires a non-local character and it is natural to apply the momentum equation, not locally and separately for the three velocity components, but in a global sense. This is done by taking the dot product of the vector equation (1b) and suitably chosen vector "test" functions, and integrating over the entire domain. The inner product $\langle \mathbf{U}, \mathbf{V} \rangle$ of two vector functions is defined as in (10) by

$$\langle \mathbf{U}, \mathbf{V} \rangle \equiv \int_{\mathscr{D}} \mathbf{U} \cdot \mathbf{V} \, dx \, dy \, dz. \tag{12}$$

Let $\mathbf{V}$ be a test function. The product of (1b) with $\mathbf{V}$ is

$$\left\langle \frac{\partial \mathbf{U}}{\partial t}, \mathbf{V} \right\rangle + \langle \boldsymbol{\omega} \times \mathbf{U}, \mathbf{V} \rangle = -\langle \nabla P, \mathbf{V} \rangle + \left\langle \frac{1}{\mathrm{Re}} \nabla^2 \mathbf{U}, \mathbf{V} \right\rangle. \tag{13}$$

Leonard used test functions $\mathbf{V}$ that satisfy the divergence-free condition (1a) and have zero normal velocity at the walls (they satisfy only the y component of (2)).

An integration by parts then shows that $\langle \nabla P, \mathbf{V} \rangle = 0$, eliminating the pressure term. Using the fact that $\mathbf{V}$ is time-independent yields

$$\frac{\partial \langle \mathbf{U}, \mathbf{V} \rangle}{\partial t} + \langle \boldsymbol{\omega} \times \mathbf{U}, \mathbf{V} \rangle = \frac{1}{\mathrm{Re}} \langle \nabla^2 \mathbf{U}, \mathbf{V} \rangle. \tag{14}$$

Unlike Leonard [16] who used (14), the formulation used here is strictly of the Galerkin type; that is, the test functions are the same as the basis functions and therefore satisfy all the boundary conditions at the wall (2). Because $\mathbf{V}$ satisfies the no-slip condition, the viscous term can be integrated by parts, yielding

$$\frac{\partial \langle \mathbf{U}, \mathbf{V} \rangle}{\partial t} + \langle \boldsymbol{\omega} \times \mathbf{U}, \mathbf{V} \rangle = -\frac{1}{\mathrm{Re}} \langle \nabla \mathbf{U}, \nabla \mathbf{V} \rangle. \tag{15}$$

Substituting the finite expansion in vector basis functions ($\mathbf{U}_n$) for $\mathbf{U}$ and using all test functions $\mathbf{V}_n = \mathbf{U}_n$, a system of nonlinear ordinary differential equations for the expansion coefficients is obtained. The time derivative and viscous terms are then represented by the matrices $\langle \mathbf{U}_n, \mathbf{U}_m \rangle$ and $\langle \nabla \mathbf{U}_n, \nabla \mathbf{U}_m \rangle$, respectively. Both the time-derivative and viscous matrices are symmetric and positive-definite. This has some computational advantages (lower storage, use of the Cholesky decomposition, simultaneous diagonalization of the two operators), and it guarantees that the numerical Stokes eigenvalues will be real and negative.

This Galerkin formulation can be derived directly from Leray's weak formulation of the analytical equations [19–21], which has been used extensively for theoretical studies of the equations and with finite-element numerical methods but apparently not with spectral methods.

The Galerkin formulation has the advantage of conserving kinetic energy in the absence of viscous terms, even after spatial discretization [2, 3] (this helps prevent numerical instabilities associated with spatial discretization). The proof uses the fact that $\mathbf{U}_1$ can be constructed as a linear combination of test-functions, and therefore does not apply with Leonard's formulation. This advantage should not be overestimated because the proof applies only if $\mathbf{U}_0$ is 0 and because most time-integration schemes do not conserve energy. Still, we probably owe our ability to use time steps up to and slightly beyond the convective stability limit (see the Appendix for definition) partly to this conservation property.

A disadvantage of the Galerkin formulations is that Chebyshev polynomials probably cannot be used in the y direction while retaining banded matrices because their weight function is singular at the wall. Moser *et al.* [13] used Chebyshev polynomials and Leonard's formulation, making the test functions less regular than the basis functions near the wall. With the vector Galerkin formulation and a regular mapping at $y = 0$ the Chebyshev weight would have to be split between the basis and test functions. This would give them both infinite derivatives at the wall, resulting in poor convergence. The possibility of "undoing" that singularity with an appropriate mapping has not been explored. Leonard and Wray [12] used Jacobi

polynomials even with the non-Galerkin method, partly to allow a proper treatment of the polar-coordinate singularity.

Although the pressure is not needed for the solution of the equations it is sometimes required for turbulence budgets or coherent-structure studies, and recovering it is not trivial. Equation (1b) can be rewritten as $\nabla P = \mathbf{A}$, where $\mathbf{A} \equiv -\partial \mathbf{U}/\partial t + \mathbf{U} \times \boldsymbol{\omega} + (1/\mathrm{Re}) \nabla^2 \mathbf{U}$. Assuming rapid decay of the vorticity, the dominant term in $\mathbf{A}$ for large y is $-\partial \mathbf{U}/\partial t$. Accordingly, the total pressure P is expanded in functions ϕ_i which have the same behavior at infinity as the scalar velocity basis functions (the regular expansion functions and the extra functions) but with no restrictions at the wall. The equation for ∇P is then written $\langle \nabla P, \nabla \phi_i \rangle = \langle \mathbf{A}, \nabla \phi_i \rangle$, yielding a sparse symmetric linear system for each wavevector. The product of $\partial \mathbf{U}/\partial t$ and $\nabla \phi_i$ is 0, and that of $\nabla^2 \mathbf{U}$ and $\nabla \phi_i$ reduces to the boundary term $\phi_i \partial^2 v/\partial y^2$ at the wall. This procedure amounts to determining P from a Poisson equation with Neumann boundary conditions and is consistent with the Galerkin formulation based on the inner product definition in (12). ∇P is not exactly equal to $\mathbf{A}$ because of truncation errors (if $\mathbf{A}$ were exactly curl-free, the vorticity equation would be solved exactly). Note that, depending on the field $\mathbf{U}_0$, the static pressure may not have the required decay at infinity to be represented using the ϕ_i functions. It is best to compute the total pressure and subtract the dynamic pressure from it to obtain the static pressure.

5.2. *Basis Functions*

Given the $+/-$ decomposition of the velocity (5), the definition of vector expansion and test functions is relatively easy [13]. The $+$ mode vector basis function $\mathbf{U}_n^+$ is given by

$$u_n^{\parallel} = \frac{i}{k} \frac{dg_n}{dy}, \qquad v_n = g_n, \qquad u_n^{\perp} = 0, \tag{16}$$

and the $-$ mode vector function $\mathbf{U}_n^-$ is given by

$$u_n^{\parallel} = 0, \qquad v_n = 0, \qquad v_n^{\perp} = h_n. \tag{17}$$

Here h_n and g_n are suitably chosen families of scalar expansion functions in y.

We next choose a mapping, which for convenience is exponential throughout the domain, not just asymptotically as $y \to \infty$:

$$\eta \equiv e^{-y/y_0}. \tag{18}$$

The parameter y_0 is a length scale of the order of the boundary-layer thickness and η is in the interval $[0, 1]$. The derivatives of a function ϕ satisfy

$$\frac{\partial \phi}{\partial y} = -\frac{\eta}{y_0} \frac{\partial \phi}{\partial \eta}. \tag{19}$$

Thus if ϕ is a polynomial in terms of η, $\partial \phi/\partial y$ is also a polynomial and of the same degree. This makes the set of polynomial basis functions described below closed

under differentiation and is a minor advantage of the exponential mapping for this problem.

To build the regular functions, let us consider the family of shifted Jacobi polynomials $Z_n(\eta) = P_n^{(0,1)}(2\eta - 1)$, where $P_n^{(0,1)}$ is as given in Abramowitz and Stegun [10]. Z_n is defined on [0, 1] with a normalization $Z_n(1) = 1$ and

$$\int_0^1 Z_n(\eta)\, Z_m(\eta)\, \eta\, d\eta = \frac{\delta_{nm}}{2(n+1)}, \tag{20}$$

where δ_{nm} is the Kronecker symbol. The expansion functions make use of the polynomials ηZ_n, which go to zero as $y \to \infty$ and which satisfy

$$\int_0^\infty (\eta Z_n)(\eta Z_m)\, dy = \frac{y_0 \delta_{nm}}{2(n+1)}, \tag{21}$$

since $dy = -y_0\, d\eta/\eta$. The shifted (0, 1) Jacobi polynomials were chosen to obtain the relationship (21). We then choose the two families of expansion functions h_n and g_n to be

$$h_n(\eta) \equiv (1-\eta)\, \eta Z_n(\eta), \qquad g_n(\eta) \equiv (1-\eta)^2\, \eta Z_n(\eta). \tag{22}$$

The h_n polynomials have a single zero at the wall since they are used for $\hat{u}^\perp$. The g_n polynomials have a double zero since they are used for $\hat{v}$, which has a double zero by continuity. Both h_n and g_n tend to 0 as y tends to $+\infty$.

The recursion relationship [10],

$$\eta Z_n = \frac{n+2}{2(2n+3)} Z_{n+1} + \frac{2(n+1)^2}{(2n+1)(2n+3)} Z_n + \frac{n}{2(2n+1)} Z_{n-1}, \tag{23}$$

and the differentiation relationship,

$$\eta(1-\eta)\frac{dZ_n}{d\eta} = -\frac{n(n+2)}{2(2n+3)} Z_{n+1} - \frac{n(n+2)}{(2n+1)(2n+3)} Z_n + \frac{n(n+2)}{2(2n+1)} Z_{n-1}, \tag{24}$$

allow us to express h_n and g_n, as well as h_n's first derivative and g_n's first two derivatives, in terms of the ηZ_m's. Higher derivatives are not needed. For instance,

$$h_n = -\frac{(n+2)}{2(2n+3)} \eta Z_{n+1} + \frac{2n^2+4n+1}{(2n+1)(2n+3)} \eta Z_n - \frac{n}{2(2n+1)} \eta Z_{n-1}, \tag{25}$$

$$\frac{dh_n}{dy} = \frac{1}{y_0}\left[\frac{(n+2)^2}{2(2n+3)} \eta Z_{n+1} + \frac{(n+1)^2}{(2n+1)(2n+3)} \eta Z_n - \frac{n^2}{2(2n+1)} \eta Z_{n-1}\right]. \tag{26}$$

Note that the multiplication by $(1-\eta)$ in (22), which was done to enforce the boundary condition, fortuitously simplifies the expression of the derivative. Equations (21), (25), and (26) allow us to compute the matrices representing the first and third terms of (15) for the $-$ modes. Both matrices are pentadiagonal. The algebra is very similar for the g_n functions, but the matrices are nonadiagonal. The cost of inverting them is $O(N)$, and they are symmetric.

The extra basis function, g_{-1}, is defined by

$$g_{-1}(\eta) \equiv 3\eta^{ky_0} + (ky_0 - 4)\,\eta Z_0 + (1 - ky_0)\,\eta Z_1. \tag{27}$$

It has a double zero at the wall and the vector function $\mathbf{U}^{+}_{-1}$ is orthogonal to the regular vector basis functions, except for the few that involve ηZ_0 or ηZ_1. We could have combined $\eta^{ky_0} = e^{-ky}$ with any two ηZ polynomials. Figure 1 is a plot of the first few g_n functions versus y, with $ky_0 = 0.4$. The extra function g_{-1} stands out for large values of y. As n increases g_n has more and more zeroes within $[0, \infty)$; the position of the zeroes roughly indicates the region where good resolution is available.

One difficulty with the extra function in method A is that if ky_0 is an integer, the extra function is not linearly independent of the regular basis functions. This makes the matrix in the first term of (15) singular. Moreover, if ky_0 is close to an integer or significantly larger than 1, the matrix becomes ill-conditioned because the regular functions can approximate the extra function too well. As a result, computer roundoff errors become excessive. To avoid this, and considering that when the extra function is very close to the regular functions it does not improve the accuracy, the extra function is not included unless ky_0 is small enough and sufficiently different from an integer. Currently we include it only if ky_0 is in one of two "windows": (0,0.9995) and (1.0005,1.85). These numbers were arrived at by examining the condition number of the matrices, and by trial-and-error (using mixed 32- and 64-bit precision).

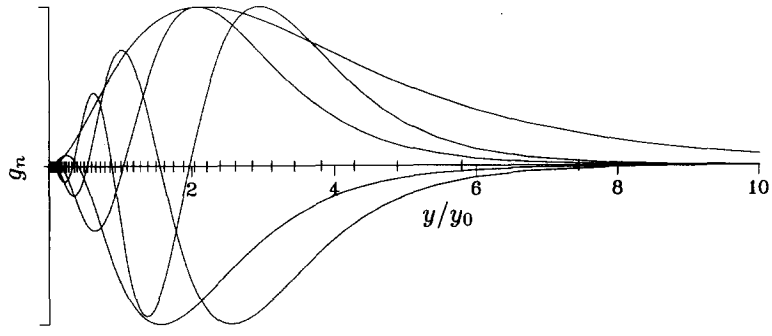

FIG. 1. Basis functions g_{-1} to g_3 of method A, with $ky_0 = 0.4$ and Gauss quadrature points with 100 points.

5.3. *Quadratures*

The solution of the momentum equation (15) requires the evaluation of various integrals. Integrals of the type $\langle \mathbf{U}, \mathbf{V} \rangle$ and $\langle \nabla \mathbf{U}, \nabla \mathbf{V} \rangle$, which enter the matrices, are computed exactly using the definitions of g_n and h_n and the properties of the Z_n polynomials. The integral $\langle \omega \times \mathbf{U}, \mathbf{V} \rangle$ is evaluated by Gauss quadrature as discussed in Section 4. In the polynomial direction the Gauss quadrature points and weights are as defined in Abramowitz and Stegun [10, p. 888]. We use the Gauss–Radau method based on the Legendre polynomials. This places a quadrature point at the wall, which is slightly wasteful compared with a pure Gauss method, but is convenient when the wall value of a quantity, such as the shear stress, is needed. Again, the number of points is $\frac{3}{2}$ as large as the number of polynomials and the quadratures are highly accurate (exact in the absence of extra basis functions). The Gauss quadrature points are indicated by ticks on the axis in Fig. 1. They are seen to cluster near the wall and be very sparse for y beyond about $5y_0$.

5.4. *Accuracy Tests*

The accuracy of the method was first tested by approximating typical mean velocity profiles: the solutions to Stokes' first problem, the Blasius equation, and the laminar sink flow [15]. The reference solution for the Blasius equation was obtained by fourth-order Runge–Kutta integration with a large number of steps. The relative error in the slope at $y = 0$ is plotted in Fig. 2 as a function of the num-

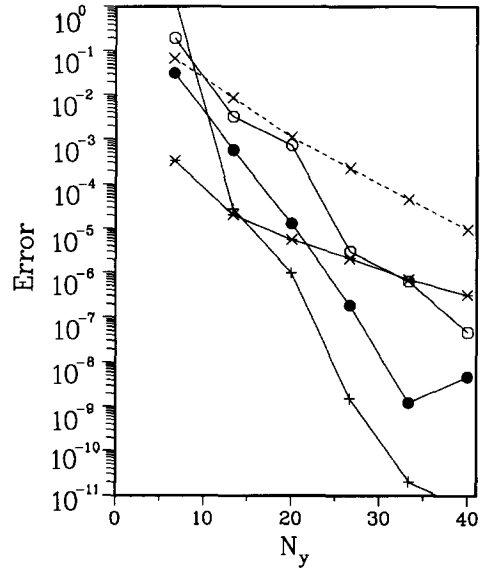

FIG. 2. Relative error in numerical solutions as a function of the number of polynomials. ● Stokes layer; ○ Blasius layer; * sink flow; + Orr–Sommerfeld equation, using the extra function; × Orr–Sommerfeld equation, omitting the extra function.

ber of polynomials. Very fast convergence is observed for the first two cases (which behave like error functions as $y \to \infty$); the convergence is only moderately fast for the sink flow. This is expected from the analysis in Section 3 because in the sink flow the vorticity decays exponentially at a slow rate. These tests do not involve the extra functions.

To test the method with extra functions, the Orr–Sommerfeld equation was also solved. Figure 3 is a plot of the spectrum for the Blasius flow at its critical condition ($\mathrm{Re}_{\delta^*} = 519.06381$ and $k\delta^* = 0.303773$, where δ^* is the displacement thickness) with 26 and 53 polynomials. The complex velocities (c_r, c_i) are plotted; c_r is the phase velocity and c_i the growth rate. The principal eigenvalue is neutrally stable. Its convergence is also shown in Fig. 2 and is very fast. A relative error of 10^{-6} in the phase velocity is obtained with 22 polynomials. Orszag [11] needed 42 Chebyshev polynomials to achieve the same accuracy (better accuracy may be obtained with the algebraic mapping by using only the odd Chebyshev polynomials, [22]). The best value of y_0 is about $2\delta^*$ and the error is not very sensitive to y_0. The convergence without the extra function g_{-1} is also plotted for comparison and is much slower, as expected and in agreement with results in [5, 8, 11].

In addition to a few discrete eigenvalues, the numerical spectra in Fig. 3 show a string of eigenvalues that starts at the point with complex velocity (1, 0) and extends to large negative values of the imaginary part. As the number of polynomials is increased this string becomes denser and slowly converges to the $c_r = 1$ axis. Grosch and Salwen [23] (see also [24]) showed that the exact spectrum includes a continuous line on that axis and that the corresponding eigenfunctions behave like sine waves as $y \to \infty$. Such functions cannot be well approximated by the basis

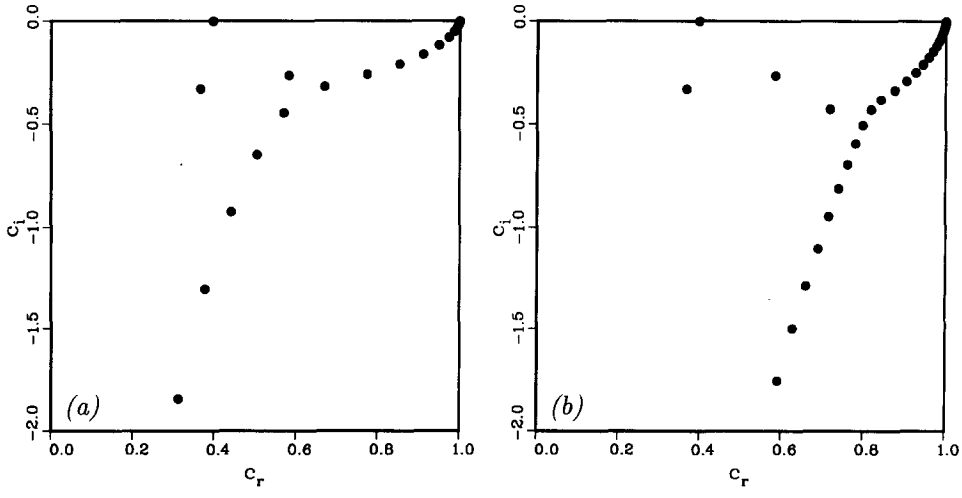

FIG. 3. Spectrum of Orr–Sommerfeld equation, in Blasius flow: (a) with 26 polynomials; (b) with 53 polynomials.

functions that were chosen, since these tend to 0 as $y \to \infty$ (Fig. 1). This explains why the convergence to the continuous part of the spectrum is so slow. These eigenfunctions are not relevant when the activity originates in the boundary layer since they do not satisfy (3). In any case the representation of the continuous spectrum, while not very accurate, is not abnormal and does not cause instabilities.

6. Method B: Mixing Layers and Wakes

In this section the Navier–Stokes equations (1) in an infinite domain $(-\infty, \infty)$ in y are considered with boundary conditions (3) and (4). The method to be described here can be cast in terms of the divergence-free expansions used in Section 5; however, because of the lack of solid boundaries a vorticity formulation is more natural and will be used for most of the presentation. The connection to divergence-free expansions will be briefly discussed in Section 6.3.

The vorticity equation, obtained from the curl of the Navier–Stokes equation (1b), can be written as

$$\frac{\partial \boldsymbol{\omega}}{\partial t} + \nabla \times (\boldsymbol{\omega} \times \mathbf{U}) = \frac{1}{\mathrm{Re}} \nabla^2 \boldsymbol{\omega}. \tag{28}$$

The boundary conditions are that the vorticity tends to 0 as $|y| \to \infty$. Note that the three components of the vorticity equation are redundant since all terms in the equation have zero divergence; that is, no gradient term (pressure) appears in response to the vorticity being divergence-free. Because of this we may choose to solve any two of the equations and obtain the third component from the divergence-free condition. After Fourier transforming, the $+/-$ decomposition can be applied and we choose to solve for $\hat{\omega}^{\perp}$ and $\hat{\omega}_y$. The other component of vorticity can be easily computed from (8). Recall that the $k = 0$ mode is treated differently ($\hat{u}$ and $\hat{w}$ are solved for). Velocity can be obtained from the vorticity by solving (9).

6.1. *Vorticity Basis Functions*

By considering the Fourier transformed vorticity equation, and taking advantage of the $+/-$ decomposition of the vorticity, the representation of the solution is reduced to the representation of two scalar functions of y (i.e., $\hat{\omega}_y$ and $\hat{\omega}^{\perp}$) for each wavenumber pair (k_x, k_z). Since all vorticity components satisfy the same boundary conditions at $\pm\infty$, the same expansion functions can be used for both vorticity components.

As discussed in Section 2, we begin by choosing a mapping of the infinite domain in y to a finite domain $[-1, 1]$ in η:

$$\eta \equiv \tanh(y/y_0). \tag{29}$$

The parameter y_0 is a length scale of the order of the shear layer thickness.

Derivatives with respect to y can be expressed in terms of derivatives with respect to η:

$$\frac{\partial \phi}{\partial y} = \frac{1-\eta^2}{y_0} \frac{\partial \phi}{\partial \eta}. \tag{30}$$

Note that if ϕ is a polynomial in η of degree N then $\partial\phi/\partial y$ is a polynomial of degree $N+1$. Thus, the polynomials are not closed with respect to diferentiation and a truncation will be required in evaluating the viscous terms. Also, $\omega^{||}$ will be a polynomial of degree one higher than $\hat{\omega}_y$ to ensure a divergence-free vorticity field.

Asymptotically η behaves as $\pm(1-2e^{\mp 2y/y_0})$ as $y \to \pm\infty$. Since the vorticity is assumed to decay at infinity like $e^{-K|y|}$, where $Ky_0/2$ is large, it can be accurately represented as a polynomial in η. The (1, 1) Jacobi polynomials, $P_n^{(1,1)}$, are selected as the building blocks for the basis functions [10]. Their orthogonality relationship is:

$$\int_{-1}^{1} P_n^{(1,1)}(\eta)\, P_m^{(1,1)}(\eta)(1-\eta^2)\, d\eta = \delta_{nm} \frac{8(n+1)}{(2n+3)(n+2)}. \tag{31}$$

The basis functions R_n are defined as

$$R_n(\eta) = (1-\eta^2)\, P_n^{(1,1)}(\eta), \tag{32}$$

which ensures that the vorticity is zero at $\eta = \pm 1$. The Jacobi polynomials and hyperbolic tangent mapping were chosen so that when expressed as functions of y, the R_n would be orthogonal on $(-\infty, \infty)$, i.e.,

$$\int_{-\infty}^{\infty} R_n(y)\, R_m(y)\, dy = y_0 \delta_{nm} \frac{8(n+1)}{(2n+3)(n+2)}. \tag{33}$$

This minimizes the bandwidths of the matrices representing the Laplacian (they are tridiagonal). In addition, the matrix associated with the time derivative is diagonal so fewer matrix solutions will be required in an explicit time advance scheme than in an implicit scheme (this is not true in method A or in those of [12–14]). The (1, 1) Jacobi polynomials satisfy a recursion relationship and a differential relationship [10] which allow us to write the derivative of R_n with respect to y as

$$\frac{dR_n}{dy} = \frac{n+1}{y_0(2n+3)} [(n+1)\, R_{n-1} - (n+3)\, R_{n+1}]. \tag{34}$$

By applying (34) twice, the second derivative can be written in the form

$$\frac{d^2 R_n}{dy^2} = \frac{1}{y_0^2} (\alpha_n R_{n+2} + \beta_n R_n + \gamma_n R_{n-2}), \tag{35}$$

where α_n, β_n, and γ_n are rational numbers depending on n. These relations are valid for $n \geqslant 0$ defining $R_{-2} = R_{-1} = 0$.

6.2. *Velocity Representation and Extra Functions*

Given the vorticity expressed as a finite expansion in R_n, the velocity must be determined to compute the nonlinear terms in (28). With the help of (9a), $\hat{u}^\perp$ is obtained directly from $\hat{\omega}_y$. A Poisson equation (9b) must be solved to obtain $\hat{v}$. Let $\hat{\nabla}^2$ be the operator $(d^2/dy^2 - k^2)$; then

$$\hat{\nabla}^2 \hat{v} = ik\hat{\omega}^\perp = ik \sum_{j=0}^{N} a_j R_j, \tag{36}$$

where the a_j are expansion coefficients for $\hat{\omega}^\perp$. Since $\hat{v}$ goes like $e^{-k|y|}$ (11) (or $ye^{-k|y|}$ for integer $y_0 k/2$) for large $|y|$, extra expansion functions besides the R_j's will be needed for $\hat{v}$.

If the functions Γ_n defined by

$$\hat{\nabla}^2 \Gamma_n = R_n \tag{37}$$

were available, $\hat{v}$ could be obtained immediately by superposition. Unfortunately, the Γ's depend on the wavenumber k and it would be impractical to compute and store them all. However, this is not necessary. Since the Laplacian is a linear operator with a unique inverse in our space of functions, the expression for the second derivative of R_n (35) is also valid for Γ_n. The following relation between the Γ's and the R's is thus obtained (with definition (37)):

$$R_n = \frac{1}{y_0^2} (\alpha_n \Gamma_{n+2} + (\beta_n - y_0^2 k^2) \Gamma_n + \gamma_n \Gamma_{n-2}) \tag{38}$$

(note that β_n is always negative). If m and l are integers of the same parity (i.e., both even or both odd), Eq. (38) evaluated for $n = 0, 1, ..., \max(m, l)$ can be manipulated to express Γ_m as a constant times Γ_l plus a polynomial in η of order $\max(m, l)$ and the same parity. Therefore, if two of the Γ's (one odd and one even) are included in the expansion along with the R_j's and if $\hat{\omega}^\perp$ has a finite representation as in (36), then the velocity $\hat{v}$ can be represented exactly, without computing and storing *all* the Γ's. The two Γ's needed for this exact representation play the role of extra functions in that they decay like $e^{-k|y|}$ (if $ky_0 < 2$) as opposed to $e^{-2|y|/y_0}$. Two extra functions are needed since the constants A in (11) are independent for $y \to -\infty$ and $y \to +\infty$.

The choice of which Γ's to use for the extra expansion functions is governed by the conditioning of the system of linear equations relating the expansion coefficients of $\hat{v}$ to those of $\hat{\omega}^\perp$ (see (40) below). The most convenient choices for extra expansion functions are (Γ_0, Γ_1) and (Γ_{N-1}, Γ_N), since they are at either end of the range of n. If Γ_0 and Γ_1 are used, then the resulting set of equations are stiff for $y_0 k > \rho$, where ρ depends on N and is of order 1. On the other hand, if Γ_{N-1} and

Γ_N are used, ill-conditioning becomes a problem for $y_0 k < \sigma$, where σ depends on N and is less than 0.1 (this was determined computationally). For the problems usually simulated with this method $y_0 k_{\min} > 0.1$ so Γ_{N-1} and Γ_N are used as extra functions. However, if a method were needed for determining $\hat{v}$ that was valid for any $y_0 k$ and any N, four extra functions (i.e., Γ_0, Γ_1, Γ_{N-1}, and Γ_N) could be used along with Eq. (38) for $n = 2, 3, \ldots, N-2$. As an example, the first four expansion functions and Γ_0 and Γ_1 for $y_0 k = 0.8$ are plotted in Fig. 4. The two extra functions Γ_n are marked by their slow decay at large y.

As stated above, two extra expansion functions are used in the current method; thus the expansion for $\hat{v}$ is

$$\hat{v}(y) = c_{N-1}\Gamma_{N-1}(y) + c_N \Gamma_N(y) + \sum_{j=0}^{N-2} c_j R_j(y). \tag{39}$$

By manipulating Eq. (35) the equations relating c_j to a_j can be obtained; they are

$$ika_j = \frac{1}{y_0^2} \begin{cases} \alpha_{j-2} c_{j-2} + (\beta_j - y_0^2 k^2)\, c_j + \gamma_{j+2} c_{j+2}, & \text{if } j \leqslant N-2; \\ \alpha_{j-2} c_{j-2} + y_0^2 c_j, & \text{if } N-1 \leqslant j \leqslant N. \end{cases} \tag{40}$$

After taking advantage of the even/odd decoupling, the solution of this system amounts to the inversion of a diagonally dominant tridiagonal matrix. It will also be necessary to compute $\hat{u}^{\parallel} = (i/k)\, \partial\hat{v}/\partial y$. This is most easily accomplished by solving

$$\hat{\nabla}^2 \hat{u}^{\parallel} = -\frac{\partial \hat{\omega}^{\perp}}{\partial y}. \tag{41}$$

In this way there is no need to compute and store the derivatives of Γ_{N-1} and Γ_N. If a_j' are the expansion coefficients for $\partial\hat{\omega}^{\perp}/\partial y$, then the expansion coefficients c_j' for

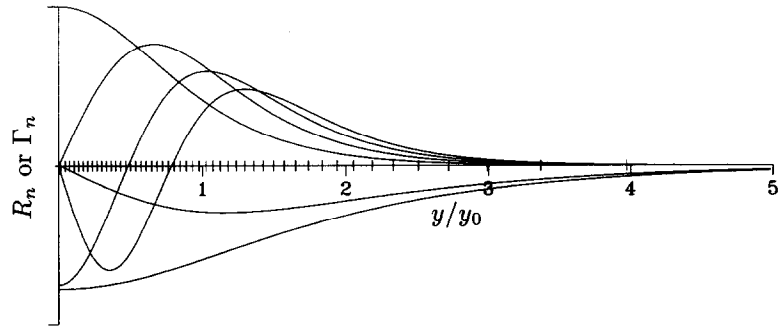

FIG. 4. Basis functions Γ_0, Γ_1, and R_0 to R_3 of method B with $ky_0 = 0.8$ and Gauss quadrature points with 100 points. Only the positive half domain is shown. All the functions are either symmetric or anti-symmetric.

$\hat{u}^{\perp}$ can be determined by substituting $-a_j'$ for ika_j and c_j' for c_j in Eq. (40). Note that if the expansion for $\partial\omega^{\perp}/\partial y$ is to terminate at order N, then a_N must be zero.

To make use of the velocity representation given by (39), the extra functions Γ_{N-1} and Γ_N must be evaluated. In computing the nonlinear terms (see Section 4) it will be necessary to evaluate the velocity on a quadrature grid, so values of the extra functions on this grid are required. Γ_n can be obtained by solving (37); the solution is

$$\Gamma_n(y) = \frac{-1}{2k} \int_{-\infty}^{\infty} e^{-k|y-y'|} R_n(y')\, dy'. \tag{42}$$

By breaking the integration domain at y, changing to mapped variables η and η' for y and y', and effecting a change of variables in the integral from η' to ξ (i.e., $\eta' = (\eta-1)\,\xi/2 + (1+\eta)/2$), the solution can be expressed as

$$\Gamma_n(\eta) = \frac{y_0}{2k} (\Phi_n(\eta) \pm \Phi_n(-\eta)),$$

$$\Phi_n(\eta) = \frac{(\eta-1)(1+\eta)^{y_0k/2}}{2(3+\eta)^{y_0k/2}} \times \int_{-1}^{1} (1+\xi)^{y_0k/2} \frac{P_n^{(1,1)}(((\eta-1)/2)\xi + ((1+\eta)/2))}{(1-(1-\eta)\xi/(3+\eta))^{y_0k/2}}\, d\xi, \tag{43}$$

where the positive sign is taken for n even, the negative for n odd. This integral can be evaluated using Gauss quadrature based on the Jacobi polynomials $P^{(0,y_0k/2)}$ [25, 26]. In this case, the $(1+\xi)^{y_0k/2}$ factor in the integrand becomes the integration weight and the remainder of the integrand is C_∞ and bounded for $-1 < \eta < 1$. The advantage of using Gauss quadrature in this context is that to compute Φ_n for n large, only $n/2$ more points are required than for Φ_0. The only numerical difficulty is that for y_0k large and η near -1, the integrand is nearly singular. It was found that for $y_0k < 20$ and fewer than 500 function evaluation points, 1000 Gauss quadrature points were adequate for one part in 10^{10} accuracy.

If y_0k is sufficiently large, the velocity $\hat{v}$ can be well represented by the regular expansion functions R_n. In this case, there is no need to use the extra functions; however, they do not cause computational problems as in method A because, although $\hat{u}$ is well resolved, Γ_N and Γ_{N-1} are not well resolved by R_n up to N. It was found that for $y_0k > 20$, Γ_0 could be represented by the regular functions to better than one part in 10^{10} accuracy for $N > 32$. Therefore, extra functions are only used for $y_0k < 20$, which has the advantage that many fewer functions need be computed and stored. Also, using the method described above to compute Γ_n becomes more difficult as y_0k gets large. When extra functions are not used, a Galerkin method based on the regular expansion functions is used to solve (9b) for $\hat{v}$. This also requires a tridiagonal matrix solution.

The computation of the Γ_n functions as described above would appear to be

quite arduous. For the largest simulations ever performed with this method ($192 \times 212 \times 128$ Fourier/Jacobi modes), extra functions were computed for 71 Fourier modes (1.2% of the modes), requiring more than two minutes of Cray Y-MP time. However, the functions need only be computed once per simulation so this constitutes a negligible fraction of the total simulation time of several hundred hours.

6.3. *Solution of the Vorticity Equation*

The vorticity equations for $\hat{\omega}_y$ and $\hat{\omega}^\perp$ are solved as independent scalar equations. The expansion for $\hat{\boldsymbol{\omega}}$ is substituted into the component vorticity equations (28) and ordinary differential equations (in time) for the expansion coefficients are obtained by the scalar Galerkin method where the test functions are R_n. The orthogonality of the basis functions and the derivative relationships (33), (34), and (35) make the integrals arising from the time derivative and the viscous terms easy to evaluate (i.e., $\int_{-\infty}^{\infty} R_n R_m \, dy$ and $\int_{-\infty}^{\infty} R_n \, d^2R_m/dy^2 \, dy$). As discussed in Section 4, the integrals arising from the nonlinear terms are computed by evaluating the velocity and vorticity on a grid and using Gauss quadrature to compute the integral. The Gauss quadrature scheme based on the $P^{(1,1)}$ Jacobi polynomials is used with $3N/2$ quadrature points and results in highly accurate quadratures (exact in the absence of extra functions). The quadrature points are marked as ticks on the axis in Fig. 4.

The scalar Galerkin method used for the y and $+$ components of the vorticity is equivalent to a divergence-free expansion formulation similar to that used in method A. The velocity $\hat{u}^\perp$ is just proportional to $\hat{\omega}_y$ and does not impact continuity. Thus this is just like a solution for the $-$ mode in the divergence-free expansion. Now consider the $+$ mode. In the vorticity equation for $\hat{\omega}^\perp$, $\hat{\nabla}^2\hat{v}/(ik)$ can be substituted for $\hat{\omega}^\perp$, resulting in a fourth-order in the space equation for $\hat{v}$. Substituting the expansion for $\hat{v}$ (39) and using the Galerkin method described above, equations for the c_j are obtained directly. These equations are equivalent to the vorticity equation solution in every way. These equations are also the same as those obtained using a divergence-free expansion formulation for the $+$ modes. The equivalent vector expansion functions are the $+$ mode vectors with R_n for $n \leqslant N$ as the y component functions. Thus, when the extra functions are used the test functions span a different space than the velocity expansion functions. Therefore the method does not correspond to the vector Galerkin formulation presented in Section 5. When the extra functions are absent the method is exactly the vector Galerkin formulation (this would not be the case with a no-slip condition).

6.4. *Test Problems*

A variety of test problems have been used to validate the numerical method described here, including the evolution of self-similar laminar velocity profiles, the computation of stability eigenvalues and eigenfunctions, and the two- and three-dimensional evolution of a mixing layer. Here the eigenvalues of the Orr–Sommerfeld equation are presented. This is a good demonstration problem because

it involves the extra functions and is easy to compute and verify. This test problem was also computed by Metcalfe *et al.* [8] and comparisons will be made with their results.

As in [8], the unstable Orr–Sommerfeld eigenvalue for the mixing layer with mean profile given by $u(y) = \tanh(y)$ was computed for three different wavenumbers using several values of the mapping parameter y_0. The computations were done using 17, 33, and 65 Jacobi polynomials, with and without the extra functions. Results of these computations are shown in Table I. The values indicated as "exact" were determined using $y_0 = 2/k$ and 200 polynomials and have converged to at least 10 digits. They agree with the three digits reported in [8]. The major difference between the cases with and without the extra functions is that without the extra functions the convergence is poor for $y_0 k < 2$. The same is true for the hyperbolic map results of Metcalfe *et al.* (see Table 1 in [8]). Also, with or without the extra functions, the accuracy suffers if y_0 is too large, since then the vortical region of the flow is not well resolved. This observation led Metcalfe *et al.* to conclude that the hyperbolic map method worked well only if y_0 is properly tuned. With the extra basis functions, convergence is good over a larger range of y_0 values, approximately the same as the range of the mapping parameter over which it is good when using the algebraic mapping in [8]. Only three digits are reported in [8], so the actual

TABLE 1

Error in Orr–Sommerfeld Eigenvalues

	$k = 0.25$			$k = 0.5$			$k = 0.75$		
Exact[a]	0.5972556424			0.3418225655			0.1365469506		
$N =$	16	32	64	16	32	64	16	32	64
y_0	Relative error with extra functions excluded								
0.5	8(−1)	6(−1)	5(−1)	7(−1)	5(−1)	3(−1)	1(+0)	6(−1)	4(−1)
1	2(−1)	1(−1)	1(−1)	1(−1)	5(−2)	3(−2)	6(−2)	2(−2)	1(−2)
2	2(−2)	1(−2)	7(−3)	2(−3)	7(−4)	2(−4)	2(−4)	2(−5)	3(−6)
4	1(−3)	1(−4)	4(−5)	1(−2)	2(−6)	3(−12)	2(−1)	4(−4)	3(−11)
8	1(−1)	1(−3)	2(−8)	5(−1)	2(−2)	3(−6)	8(+0)	2(−1)	5(−4)
y_0	Relative error with extra functions included								
0.5	5(−2)	1(−2)	6(−3)	5(−2)	2(−2)	7(−3)	4(−2)	1(−2)	5(−3)
1	2(−4)	1(−5)	2(−6)	3(−4)	5(−5)	6(−6)	2(−4)	2(−5)	2(−6)
2	2(−6)	2(−7)	3(−7)	3(−6)	7(−9)	3(−9)	1(−4)	3(−10)	6(−11)
4	1(−3)	9(−7)	1(−9)	1(−2)	2(−6)	3(−12)	2(−1)	4(−4)	1(−11)
8	1(−1)	1(−3)	2(−8)	5(−1)	2(−2)	3(−6)	6(+0)	2(−1)	5(−4)

[a] Eigenvalues are for the mixing layer with $u(y) = \tanh(y)$ and $\mathrm{Re} = 100$. Quoted are the growth rates $(x(y) = x \cdot 10^y)$ for the fastest growing temporal mode of the form $\psi(y)\, e^{ik(x-ct)}$.

magnitudes of the errors cannot be compared. Note that when using the extra functions, the error magnitudes for the current method approach roundoff level.

Another set of stability computations was performed to demonstrate the convergence of the method with increasing N. In these computations, the velocity profile was taken to be $u(y) = \mathrm{erf}(\sqrt{\pi}\, y)$ and the wavenumber k was taken to be 0.862 which is close to the most unstable wavenumber. Four Reynolds numbers and two values of y_0 were used. The results are shown in Fig. 5. When the extra functions are used the convergence is nearly exponential (straight lines on these log-linear plots). Without the extra functions, the error decreases exponentially for small N, but decays algebraically and very slowly for large N. As discussed in Section 3 this is expected because of the behavior of the velocity as $|y| \to \infty$. Note that the exponential portions of these curves follow the curves for the cases including the extra functions. The reason for this behavior is that for these small values of N the error in representing the vorticity dominates, and the treatment of the vorticity is the same in each case. Also, for all Reynolds numbers the algebraic portions of the convergence curves are the same, because this is governed by the behavior of the irrotational component of the velocity which is independent of the Reynolds number. The error level at which algebraic convergence is manifested is lower for larger y_0, while the rate of exponential convergence is slower for larger y_0. In

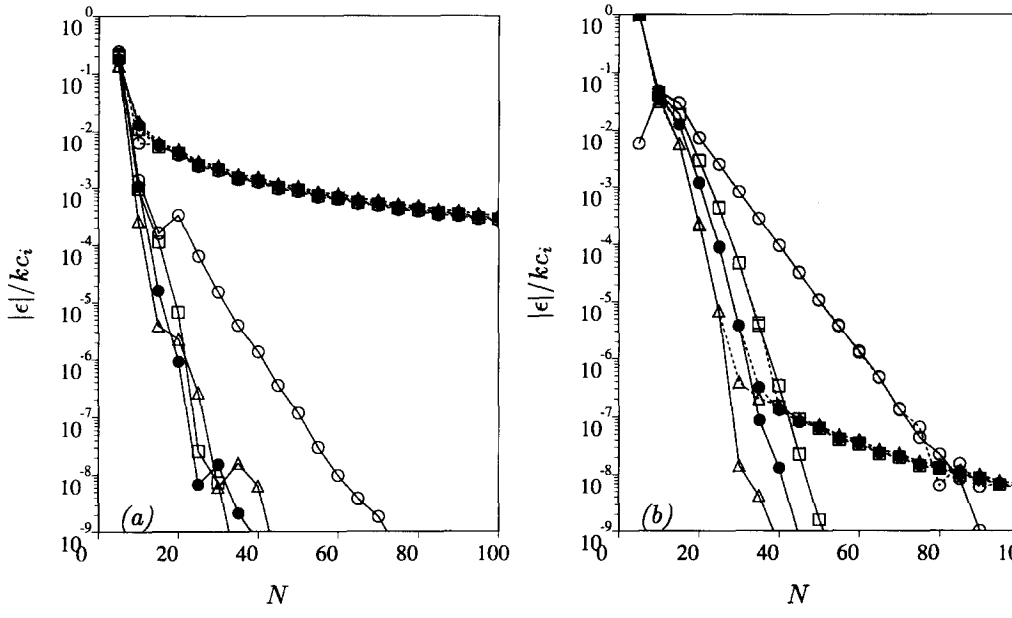

FIG. 5. Relative error in the growth rate (kc_i) of the most unstable temporally-growing disturbance of the form $\psi(y)\, e^{ik(x-ct)}$ of the mixing layer with $u(y) = \mathrm{erf}(\sqrt{\pi}\, y)$. Computations were done with (a) $y_0 = 1$ and (b) $y_0 = 2$. Results including extra functions are shown with solid lines, while results excluding extra functions are plotted with dashed lines. The Reynolds numbers are △ 125; ● 250; □ 500; and ○ ∞.

addition, the rates of exponential convergence decrease with Reynolds number (although the curves are not all well separated for $y_0 = 1$). These observations are also consistent with the expected convergence properties of the vorticity and the irrotational component of the velocity.

APPENDIX: TIME INTEGRATION

Method B uses a low-storage third-order Runge–Kutta scheme designed by A. Wray (submitted to *J. Comput. Phys.*). Method A uses a slight generalization of that scheme, in order to provide implicit treatment of the viscous term, which is presented here.

The system of equations for the unknown vector function $\mathbf{u}$ can be written as

$$\frac{\partial \mathbf{u}}{\partial t} = L(\mathbf{u}) + N(\mathbf{u}) \equiv R(\mathbf{u}), \tag{A1}$$

where L is a linear operator and N is a nonlinear operator. They do not depend explicitly on t. Typically L comprises the viscous and pressure terms and N the convection term; but any linear term can be included in either operator. In particular, for method B, $L = 0$ and we include all terms in N. With a no-slip condition, as in method A, L is stiff and requires an implicit scheme if a reasonable time step is to be used. N is always hard to linearize in a spectral method and thus requires an explicit scheme if one wants to avoid iterating. We wish to extend Wray's analysis to obtain a low-storage, hybrid implicit/explicit, three-substep scheme of highest possible order.

Let $\mathscr{D}$ and $\mathscr{E}$ be the first and second derivatives of N with respect to $\mathbf{u}$. Then $\mathscr{D}$ is a linear operator, $\mathscr{E}$ is a bilinear operator which is symmetric with respect to its arguments, and

$$N(\mathbf{u} + d\mathbf{u}) = N(\mathbf{u}) + \mathscr{D}(d\mathbf{u}) + \tfrac{1}{2}\mathscr{E}(d\mathbf{u}, d\mathbf{u}) + O(d\mathbf{u}^3). \tag{A2}$$

Thus

$$\mathbf{u}(t + \Delta t) = \mathbf{u} + \Delta t\, R(\mathbf{u}) + \frac{\Delta t^2}{2}(L + \mathscr{D})(R(\mathbf{u}))$$

$$\times \frac{\Delta t^3}{6}[\mathscr{E}(R(\mathbf{u}), R(\mathbf{u})) + (L + \mathscr{D})^2(R(\mathbf{u}))] + O(\Delta t^4). \tag{A3}$$

To achieve the desired accuracy the numerical scheme should match this Taylor expansion to third order. The scheme to advance from $\mathbf{u}_n$, at time t, to $\mathbf{u}_{n+1}$, at time $t + \Delta t$, has three substeps:

$$\mathbf{u}' = \mathbf{u}_n + \Delta t[L(\alpha_1 \mathbf{u}_n + \beta_1 \mathbf{u}') + \gamma_1 N_n] \tag{A4a}$$

$$\mathbf{u}'' = \mathbf{u}' + \Delta t[L(\alpha_2 \mathbf{u}' + \beta_2 \mathbf{u}'') + \gamma_2 N' + \zeta_1 N_n] \tag{A4b}$$

$$\mathbf{u}_{n+1} = \mathbf{u}'' + \Delta t[L(\alpha_3 \mathbf{u}'' + \beta_3 \mathbf{u}_{n+1}) + \gamma_3 N'' + \zeta_2 N'], \tag{A4c}$$

where $N_n \equiv N(\mathbf{u}_n)$, $N' \equiv N(\mathbf{u}')$, and $N'' \equiv N(\mathbf{u}'')$. For N this is Wray's scheme (for each substep it is like Euler explicit or second-order Adams–Bashforth, but with different coefficients γ and ζ). For L this is like the Crank–Nicolson scheme on each substep but again with different coefficients. This extra freedom should allow us to obtain third-order accuracy. The advantage of the scheme described here is that it needs only the minimum of storage, actually no more than the Euler explicit scheme for the present methods. A disadvantage compared with Adams–Bashforth is that there are three different implicit operators ($[1 - \Delta t\, \beta L]$ in (A4)) so it would be more costly to precompute them, preinvert them, and store them. Currently we do not precompute the operators because the time step is adjusted continually to keep the peak CFL number constant.

The general scheme (A4) has 11 unknown coefficients and must satisfy 17 equations for third-order accuracy (expand (A3) and recall that L and $\mathscr{D}$ do not commute). However, Leonard (personal communication) in a similar scheme requires

$$\alpha_1 + \beta_1 = \gamma_1, \qquad \alpha_2 + \beta_2 = \gamma_2 + \zeta_1, \qquad \alpha_3 + \beta_3 = \gamma_3 + \zeta_2, \tag{A5}$$

which mean that the length of the substeps is the same in the scheme for L and the scheme for N. This seems reasonable and it reduces the system to eight equations in eight unknowns (because the terms $L(\mathbf{u})$ and $N(\mathbf{u})$ do not get separated). From here on we replace α_1 by $\gamma_1 - \beta_1$, and so on. The equations are, for first order,

$$\gamma_1 + \gamma_2 + \gamma_3 + \zeta_1 + \zeta_2 = 1; \tag{A6}$$

for second order,

$$\gamma_3(\gamma_1 + \gamma_2 + \zeta_1) + \gamma_1(\zeta_2 + \gamma_2) = \tfrac{1}{2}, \tag{A7a}$$

$$\gamma_1\beta_1 + \gamma_1(\gamma_2 + \zeta_1) + (\gamma_2 + \zeta_1)\,\beta_2 + (\gamma_3 + \zeta_2)(\gamma_1 + \gamma_2 + \zeta_1) + \beta_3(\gamma_3 + \zeta_2) = \tfrac{1}{2}; \tag{A7b}$$

for third order,

$$\gamma_1\gamma_2\gamma_3 = \tfrac{1}{6}, \tag{A8a}$$

$$\gamma_1^2(\gamma_2 + \zeta_2) + \gamma_3(\gamma_1 + \zeta_1 + \gamma_2)^2 = \tfrac{1}{3}, \tag{A8b}$$

$$\beta_3[\gamma_3(\gamma_1 + \gamma_2 + \zeta_1) + \gamma_1\zeta_2] + \gamma_1\gamma_2(\gamma_3 + \zeta_2) + \gamma_1\gamma_2\beta_2 = \tfrac{1}{6}, \tag{A8c}$$

$$\gamma_3[\gamma_1\beta_1 + (\gamma_2 + \zeta_1)(\gamma_1 + \beta_2)] + \gamma_1\beta_1(\gamma_2 + \zeta_2) = \tfrac{1}{6}, \tag{A8d}$$

$$\begin{aligned}&[(\gamma_1 + \beta_3 + \beta_2)(\zeta_1 + \gamma_2) + (\beta_3 + \beta_1)\,\gamma_1 + \beta_3^2]\,\zeta_2 \\ &\quad + [(\gamma_1 + \beta_3 + \beta_2)\,\gamma_3 + (\beta_2 + \beta_1)\,\gamma_1 + \beta_2^2]\,\zeta_1 \\ &\quad + [(\gamma_1 + \beta_3 + \beta_2)\,\gamma_2 + (\beta_3 + \beta_1)\,\gamma_1 + \beta_3^2]\,\gamma_3 \\ &\quad + [(\beta_2 + \beta_1)\,\gamma_1 + \beta_2^2]\,\gamma_2 + \beta_1^2\gamma_1 = \tfrac{1}{6}.\end{aligned} \tag{A8e}$$

Wray had obtained (A6), (A7a), and (A8a)–(A8b) (i.e., four equations for five unknowns) and found a one-parameter family of explicit third-order schemes.

Unfortunately this nonlinear system of equations (A6)–(A8) apparently does not have a solution. We sacrificed the last equation (A8e) because it involves only the viscous term. The scheme is still third-order on the pure convection terms and on the cross-terms. There is then a one-parameter family of such schemes, as found by Wray, and the mismatch in the last equation gets as low as 0.018. A good compromise between this mismatch and the desire to have fairly even substeps is

$$\gamma_1 = \tfrac{8}{15}, \quad \gamma_2 = \tfrac{5}{12}, \quad \gamma_3 = \tfrac{3}{4}, \quad \zeta_1 = -\tfrac{17}{60}, \quad \zeta_2 = -\tfrac{5}{12},$$
$$\alpha_1 = \tfrac{29}{96}, \quad \alpha_2 = -\tfrac{3}{40}, \quad \alpha_3 = \tfrac{1}{6},$$
$$\beta_1 = \tfrac{37}{160}, \quad \beta_2 = \tfrac{5}{24}, \quad \beta_3 = \tfrac{1}{6}.$$

Presumably full third-order accuracy could be obtained with a four-substep scheme, but our main interest is in the stability of the third-order Runge–Kutta scheme (the theoretical limit is a CFL number of $\sqrt{3}$). In practice, with the help of the viscous term and the intermittency of the high-velocity conditions, peak CFL numbers up to two are routinely used. The definition of CFL used here is

$$\mathrm{CFL} \equiv \frac{2}{3}\pi \left[\frac{|u|}{\Delta x} + \frac{|v|}{\Delta y} + \frac{|w|}{\Delta z} \right] \Delta t, \tag{A9}$$

where Δx, Δy, and Δz are quadrature grid spacings, the factor of $\frac{2}{3}$ is used to account for the fact that the quadrature mesh has $\frac{3}{2}$ as many points as modes in each coordinate direction for dealiasing and the definition for the y component is purely by analogy with the Fourier directions. This translates into a CFL number of $\frac{2}{3}$ per evaluation, appreciably larger than the CFL numbers used in similar simulations with the Adams–Bashforth scheme.

Another stability advantage of the new scheme is that when the eigenvalues of L are large in magnitude, their eigenvectors are damped by a ratio approaching $\frac{87}{185}$ at each full step. In contrast, with Crank–Nicolson there is little damping since the ratio approaches -1. However, this extreme situation is not encountered in our simulations because the viscosity is small.

Acknowledgments

The authors are thankful for useful discussions at the NASA Ames Research Center with Drs. J. Buell, J. Kim, A. Leonard, P. Moin, R. Rogallo, and A. Wray.

References

1. R. S. Rogallo and P. Moin, *Ann. Rev. Fluid Mech.* **16**, 99 (1984).
2. D. Gottlieb and S. A. Orszag, *Numerical Analysis of Spectral Methods* (SIAM, Philadelphia, 1977).

3. C. CANUTO, M. Y. HUSSAINI, A. QUARTERONI, AND T. A. ZANG, *Spectral Methods in Fluid Dynamics* (Springer-Verlag, Berlin, 1987).
4. C. E. GROSCH AND S. A. ORSZAG, *J. Comput. Phys.* **25**, 273 (1977).
5. J. P. BOYD, *J. Comput. Phys.* **45**, No. 1, 43 (1982).
6. S. A. ORSZAG AND A. T. PATERA, *J. Fluid Mech.* **128**, 347 (1983).
7. A. B. CAIN, J. H. FERZIGER, AND W. C. REYNOLDS, *J. Comput. Phys.* **56**, No. 2, 272 (1984).
8. R. W. METCALFE, S. A. ORSZAG, M. E. BRACHET, S. MENON, AND J. J. RILEY, *J. Fluid Mech.* **184**, 207 (1987).
9. E. LAURIEN AND L. KLEISER, *J. Fluid Mech.* **199**, 403 (1989).
10. M. ABRAMOWITZ AND I. A. STEGUN, *Handbook of Mathematical Functions*, Appl. Math. Series, Vol. 55 (Nat. Bur. Stand., Washington, DC, 1972).
11. S. A. ORSZAG, Report 63, Flow Research Inc., Kent, WA, 1976 (unpublished).
12. A. LEONARD AND A. A. WRAY, in *8th Int. Conf. on Num. Methods in Fluid Dyn.*, edited by E. Krause (Springer-Verlag, Berlin, 1982).
13. R. D. MOSER, P. MOIN, AND A. LEONARD, *J. Comput. Phys.* **52**, 524 (1983).
14. S. K. STANAWAY, B. J. CANTWELL, AND P. R. SPALART, AIAA Paper 88-0318, 1988 (unpublished).
15. H. SCHLICHTING, *Boundary Layer Theory*, 7th ed. (McGraw–Hill, New York, 1979).
16. A. LEONARD, *Bull. Amer. Phys. Soc.* **26**, 1247 (1981).
17. P. R. SPALART, *J. Fluid Mech.* **187**, 61 (1989).
18. T. A. ZANG, *Appl. Num. Math.*, submitted.
19. O. A. LADYZHENSKAYA, *The Mathematical Theory of Viscous Incompressible Flow*, 2nd ed. (Gordon & Breach, New York, 1969).
20. J. G. HEYWOOD, *Indiana Univ. Math. J.* **29**, No. 5, 639 (1980).
21. R. TEMAM, *Navier–Stokes Equations and Non-linear Functional Analysis*, NSF-CMBS Monograph 41 (SIAM, Philadelphia, PA, 1983).
22. P. R. SPALART, *Contemp. Math.*, Vol. 28, p. 315, edited by J. E. Marsden (Am. Math. Soc., Providence, RI, 1984).
23. C. E. GROSCH AND H. SALWEN, *J. Fluid Mech.* **87**, No. 1, 33 (1978).
24. B. N. ANTAR AND J. A. BENEK, *Phys. Fluids* **21**, No. 2, 183 (1978).
25. G. H. GOLUB AND J. H. WELSCH, *Math. Comput.* **23**, 221 (1969).
26. A. GHIZZETTI AND A. OSSICINI, *Quadrature Formulae* (Birkhäuser, Basel/Stuttgart, 1970).